JOURNAL OF CATALYSIS 145, 344–355 (1994)

Synthesis of High Surface Area Molybdenum Nitride in Mixtures of Nitrogen and Hydrogen

R. S. Wise and E. J. Markel[1]

Department of Chemical Engineering, University of South Carolina, Columbia, South Carolina 29208

Received January 21, 1993; revised September 8, 1993

The production of high surface area (150 m^2/g, passivated) unsupported γ-Mo_2N by temperature programmed reaction of MoO_3 powder with mixtures of H_2 and N_2 is reported. The addition of 1290 ppm H_2O or more to the synthesis gases leads to reduced product surface areas by either hydrothermal sintering or lattice fluidization mechanisms. Reduced surface areas in syntheses with lower N_2/H_2 space velocities and higher temperature ramping rates are attributed to increased concentrations of H_2O evolved by reaction. Elevated H_2O concentrations increase the temperature required for solid reduction. Observed reaction intermediates include MoO_2, Mo, and an unidentified molybdenum oxide, hydroxide, or hydrate. Intermediates in topotactic syntheses exhibited intermediate surface areas (up to 60 m^2/g). A thermodynamic analysis indicates that, in most cases, the intermediate solids are not in equilibrium with the gas phase and that solids may be reduced completely to Mo before nitridation. It is concluded that the rate of the gas/solid reaction rate is determined primarily by the rate of oxygen and nitrogen diffusion in the solid lattice but that competitive adsorption of H_2O and H_2 also influences the rate of the gas/solid reaction.

INTRODUCTION

Recent studies have reported the production of high specific surface area γ-Mo_2N (up to 170 m^2/g, passivated) in temperature programmed reactions of MoO_3 and flowing NH_3 (1, 2). The high specific surface area of this material makes it a particularly promising compound for heterogeneous catalysis. γ-Mo_2N prepared by this method has been studied as a catalyst for NH_3 synthesis (3), ethane hydrolysis (4), hydrodenitrogenation (5, 6), CO hydrogenation (5), and hydrodesulfurization (1). γ-Mo_2N also finds use in hardened, high temperature alloys. A related compound, MoN, has been studied for its superconductive properties, and has a theoretical critical temperature near 30 K (7). γ-Mo_2N itself has a critical superconducting temperature of 5.0 K (8).

In a previous study of topotactic Mo_2N synthesis (9), we found that the NH_3 feed gas can catalytically decompose by as much as 99.88% during temperature programmed reaction. To more fully understand the NH_3 synthesis reaction and to explore new reaction chemistries, we report here an investigation of the MoO_3 reduction in mixtures of H_2 and N_2. In this work, a new method for the synthesis of high surface area (up to 150 m^2/g, passivated) γ-Mo_2N was found. This synthesis route offers several advantages over the NH_3 synthesis, especially for large scale production of high surface area γ-Mo_2N.

LITERATURE REVIEW

The synthesis of high surface area Mo_2N by reaction of MoO_3 and NH_3 has been reviewed previously (1–5), but no previous synthesis of high surface area Mo_2N in N_2/H_2 mixtures is reported. Related reactions of molybdenum oxides and H_2 are known. Bertrand and Dufour studied the topotactic isothermal reduction of MoO_3 in water-free, flowing H_2 at 100 Torr (1 Torr = 133.3 N m^{-2}). Low temperatures (723–743 K) were used to avoid complete reduction of the oxides to Mo metal and water-free H_2 was used because slight traces of water have been shown to enhance MoO_3 sublimation by the formation of volatile hydrates (10). The reaction products were found to be MoO_2 and H_2O:

$$MoO_3 + H_2 = MoO_2 + H_2O. \qquad [i]$$

Using selected area electron diffraction it was shown (11) that the following structural relationships exist during the topotactic reduction: $[100]MoO_2 \| [010]MoO_3$, $[122]MoO_2 \| [100]MoO_3$, and $[12\bar{2}]MoO_2 \| [001]MoO_3$. The authors also reported an activation energy of 19 ± 2 kcal/mol for this reduction.

In an earlier study, Hillis *et al.* (12) prepared MoO_2 by reduction of MoO_3 at 793 K in H_2O-laden H_2 at 1 atm (dewpoint 341 K). MoO_2 produced in this manner had a low surface area (0.8 to 1.2 m^2/g) and is not expected to be topotactic. It was shown that no chemisorption of N_2

[1] To whom correspondence should be addressed.

0021-9517/94 $6.00

occurs on the MoO_2 in a temperature range 273 K to 823 K. Reduction of MoO_3 in water-free H_2 at 773 K led to formation of Mo metal and an unidentified compound in addition to MoO_2.

Hillis *et al.* (12) also studied the isothermal reduction of low surface area MoO_2 in water-free flowing atmospheric H_2 at 788K:

$$MoO_2 + 2H_2 + Mo + 2H_2O. \qquad [ii]$$

The reaction product was identified by X-ray diffraction as a mixture of Mo metal and the low surface area MoO_2 starting material. The reduction kinetics were such that a period of 30 hr was required for a 30% conversion to Mo. At equilibrium, it is expected that all of the dioxide will be converted to the metal (13). Reduction of the low surface area MoO_2 in water free H_2 did not form the unidentified compound found in corresponding trioxide reductions. The specific surface area of the MoO_2/Mo product mixtures increased linearly from 2 m^2/g to a final value of 50 m^2/g.

Kinetic data for catalytic ammonia synthesis using these MoO_2/Mo mixtures were also reported (12). The NH_3 concentration in the gas phase did not exceed 1.5 ppm during these syntheses. It was determined that ammonia synthesis was catalyzed only by the Mo metal present in Mo/MoO_2 mixtures and that a surface layer of N_2 or a nitrogen compound significantly enhanced the rate of NH_3 synthesis. The rate of NH_3 synthesis was vastly decreased when 17 Torr of H_2O was introduced into the stoichiometric, atmospheric pressure H_2/N_2 feed. Activity was restored by degassing the MoO_2/Mo catalyst.

Some nitridation of the MoO_2/Mo catalyst to γ-Mo_2N occurred in these reactions as well. It was found that the nitride would form only in syntheses in which the partial pressure of N_2 was higher than 30 Torr (the dissociation pressure of Mo_2N at 773). Complete conversion of a 90% Mo/MoO_2 mixture to γ-Mo_2N was achieved by reaction with 760 Torr N_2 at 583 K for 20 hours. Surface areas of the nitride phase were less than those of the MoO_2/Mo phase. The authors were able to regenerate the Mo metal phase by hydrogen reduction of the nitride.

METHODS

All H_2/N_2 mixtures (Matheson, UHP N_2 (99.9995%) or H_2 (99.9995%)) were mixed and metered using needle valves and rotameters (Linde Specialty Gases). Water was added to gaseous mixtures as required by syringe pump injection. MoO_3 powder (0.5 gram, Johnson Matthey, 99.99%) was loaded in 4 mm ID × 8 mm OD × 1 m quartz tube reactors and held in place by a porous quartz disk (10 mm pores) fused in the tube. The loaded reactors were placed in a tube furnace and connected to the gas feed system in a downflow geometry. After allowing a brief period for stabilization of the gas flows, the temperature ramping program was initiated.

Following reaction, nitrogen gas flow was maintained as the reaction vessel was removed from the furnace to cool. Most of the high surface area materials were air sensitive and would oxidize violently if exposed to air immediately following reaction. Caution should be exercised when handling the unpassivated samples, especially in the presence of hydrogen. Careful purging of hydrogen using an inert gas such as nitrogen is recommended before exposure of the system to air. Air stable samples were formed by allowing air to diffuse into the reactor tube through 0.5-m-long $\frac{1}{4}$-in. ID tubing for a period of 24 hr. We have shown (14) using diffuse reflectance FTIR that passivated γ-Mo_2N forms an amorphous MoO_2 surface layer and the slow rate of passivation is required due to the exothermic nature of the oxidation. Volpe and Boudart (2) have shown that substantial losses in surface area accompany the passivation procedure.

During some reactions, the feed and effluent gases were analyzed by gas chromatography. Sample injection was performed by a pneumatically actuated sampling valve on the reactor effluent stream. A 2 m by $\frac{1}{8}$ in. diameter stainless steel Porapak N column (AllTech Associates) was used for separation of H_2O, N_2, and NH_3 in flowing helium (Matheson, 99.9995%). The column was installed in a Hewlett Packard 5890A gas chromatograph equipped with a thermal conductivity detector (TCD). Automatic gas sampling and data acquisition were controlled by an IBM PC/AT computer equipped with an Interactive Microware package A/D converter, PC/AT logic board, and software. Samples were typically taken every 350 sec. a rate limited by the retention time of water in the column.

Solids were analyzed using a Rigaku X-Ray Diffractometer (model D-max B) equipped with a Cu source and a grating monochromator system for rejection of spurious lines. Samples were ground as required and mounted on backless aluminum sample holders using an amorphous adhesive tape. All data were compared to JCPDS catalog values (15) for identification.

The X-ray diffraction peak widths may be related to the size of a crystallite in any particular $\langle hkl \rangle$ direction (16) using the Scherrer equation,

$$d_{hkl} = K\lambda/b \cos \theta, \qquad [iii]$$

where b is the corrected peak width at half maximum in terms of deflection angle (2θ), λ is the incident radiation wavelength, θ is the angle of diffraction, d_{hkl} is the dimension of coherently reflecting domains in the (hkl) direction, and K is taken as unity. The corrected value b should be distinguished from B, the measured angular width at half maximum (FWHM). The value of b may be obtained using

TABLE 1

Effect of Space Velocity on Product Surface Area (933 K Syntheses)

Sample	Gas composition (% H_2)	Total space velocity (hr^{-1})	Surface area (m^2/g)
SVF01	84.9%	259,000	151.
SVF02	76.8%	141,000	124.
SVF03	76.4%	107,000	110.
SVF04	82.3%	99,500	119.
SVF05	66.9%	43,800	31.1
SVF06	76.3%	22,400	23.6
SVF07	83.9%	21,100	14.4

Warren's formula for Gaussian type curves, $b^2 = B^2 - b_0^2$, where b_0 is a measure of the instrumental broadening obtained from the FWHM of a material with partaicle dimensions in excess of 3000Å (17). It should also be mentioned here that the value of d_{hkl} is used as a relative measure of lattice extent in the $\langle hkl \rangle$ direction only. If d is defined as the cube root of volume the value of K is a function of the crystallite orientation and particle morphology. The average crystallite diameter may also be estimated from surface area by the relation

$$S_g = 6/\rho\, d_p. \qquad [iv]$$

BET surface area analysis and pore volume measurements were performed using a Micromeritics 2700 dynamic adsorption analyzer. The N_2/He mixtures used in adsorption measurements were prepared in the laboratory by mixing commercial gases (Matheson N_2, 99.9995%, and He, 99.9995%) in a Sierra CalBox dual-channel electronic mass flow controller. An integrating thermal conductivity detector was used to determine test gas composition during adsorption/desorption. Adsorption was carried out at liquid nitrogen temperatures.

RESULTS

In this work we report the first temperature programmed synthesis of high surface area γ-Mo_2N from H_2/N_2 mixtures and MoO_3. The synthesis conditions were chosen to be similar to those of the NH_3-based synthesis: a gas space velocity of 260,000 hr^{-1} and a temperature ramping rate of 0.6 K/min were used. The final reaction temperature was chosen to match the estimated operating temperature of the bed at the end of the NH_3 reaction, assuming complete endothermic decomposition of the NH_3 gas. The H_2/N_2 ratio was chosen to be between that of decomposed NH_3 and the stoichiometric ratio of 12 required for formation of γ-Mo_2N from MoO_3. These synthesis conditions (Table 1) produced γ-Mo_2N with the highest specific surface area of this work (151 m^2/g, passivated).

Space Velocity Effects

It has been reported that reduced NH_3 space velocities lead to lower product specific surface areas (1). The sample series SVF (Table 1) was prepared to determine the effect of space velocity on the N_2/H_2 product specific surface area at 933 K. All samples were prepared with identical temperature ramping programs of 0.6 K/min and identical reactant bed volumes. As in the NH_3 synthesis, the specific surface areas were found to increase with total space velocity of the H_2/N_2 feed gas.

Temperature Ramping Rate Effects

A temperature ramping rate of 0.6 K/min was used during most syntheses in this work. It has been shown that temperature ramping rates in excess of 0.6 K/min result in reduced specific surface areas (1, 2) in the NH_3 synthesis. The sample series TRR (Table 2) was prepared to measure the effect of the temperature ramping rate on the surface area of the N_2/H_2 product. These samples were prepared using an intermediate space velocity of 100,000 hr^{-1}, with a 5/1 H_2/N_2 ratio. It is observed that increases in the temperature ramping rate lead to reduced specific surface area γ-Mo_2N.

Feed Gas Composition Effects

Sample series PG (Table 3) was prepared to examine the effect of the H_2/N_2 ratio on Mo_2N surface area. It was found that hydrogen-rich mixtures yielded the highest surface area Mo_2N. A hydrogen-lean mixture produced a mixture of low surface area MoO_2, Mo_2N, and Mo. While no changes in solid composition were observed for reaction in pure nitrogen, reaction in pure hydrogen gave nearly complete conversion to high surface area Mo at only 773 K. Scherrer calculations indicate the Mo particles are approximately 4 nm in diameter but the observed surface areas are lower than expected of metal spheres. Traces of an unknown material with a lattice spacing at

TABLE 2

Effects of Temperature Ramping Rate on Product Surface Area

Sample	Ramp rate	Surface area (m^2/g)	Average water content[a]
TRR01	0.6 K/min	119.	1490 ppm
TRR02	1.0 K/min	76.9	1760 ppm
TRR03	2.0 K/min	45.1	2630 ppm

[a] Average water content during reduction obtained by averaging measured effluent water concentration from the onset of MoO_3 reduction until the end of temperature-programmed reaction.

TABLE 3

Effect of Synthesis Gas Composition on Product Composition and Surface Area

Sample	H_2	N_2	Space velocity	Surface area	Product	Temp.
PG01	0%	100%	32,600 hr^{-1}	3.0 m^2/g	MoO_3	933 K
PG02	12.5%	87.5%	107,000 hr^{-1}	10. m^2/g	MoO_2/γ-Mo_2N/Mo	933 K
PG03	30%	70%	100,000 hr^{-1}	37.4 m^2/g	γ-Mo_2N	933 K
SVF04	82.3%	17.7%	99,500 hr^{-1}	119 m^2/g	γ-Mo_2N	933 K
PG04	100%	0%	264,000 hr^{-1}	73.0 m^2/g	Mo[a]	773 K

[a] Smaller quantities of I205 also observed in this synthesis.

205 pm were also observed in the hydrogen synthesis. This material was previously observed in NH_3 syntheses and was ascribed to an oxynitride species (2). For brevity, this compound is identified as I205 throughout the remainder of this report.

Effect of H_2O in Feed Gas

In an effort to better understand the effect of hydrothermal sintering on the reaction mechanism, we repeated several of our syntheses with a fixed water potential in the feed gas. Table 4 and Fig. 1 summarize the results of these experiments. This synthesis series (WC) was produced using identical reducing conditions to those for sample SVF04, e.g., a space velocity of 100,000 hr^{-1}, a temperature ramping rate of 0.6 K/min, and a 5/1 H_2/N_2 ratio. It was found that a bulk water content of 1294 ppm inhibited the development of high surface area γ-Mo_2N and water concentrations greater than 2782 ppm resulted in the formation of Mo. Scherrer analysis of the Mo peaks indicates large particle diameters (>1000 Å) and very low Mo surface areas. The relative intensities of the primary Mo peak (near 44°) are greater for syntheses with higher water concentrations (Fig. 1). The average effluent water content during reduction increases with feed gas water content. In fact, the difference between the effluent and feed gas water contents increases as well. This effect is due to the shortening of the period over which reduction occurs as the feed water content is increased: at high feed water contents, reduction is delayed so that reactions producing water occur quickly at high temperature (18). Thus, high effluent water contents are observed.

Effluent H_2O Analyses

Given the observation that even 1294 parts per million of water could influence the Mo_2N surface area, the effluent gas for all samples in reaction series TRR was analyzed for water content throughout the temperature programmed reaction (Table 2, Fig. 2). During temperature programmed synthesis at 0.6 K/min, the reduction of MoO_3 to MoO_2 is clearly seen as a sharp spike of evolved H_2O near 613 K. The further reduction to γ-Mo_2N is not clearly defined, but a broad maximum in off-gas water concentration is seen to occur near 793 K. The average H_2O content (Table 2) was calculated from the gas chromatograph data over the temperatures at which reaction was observed. Similar patterns are observed at higher ramping rates (Figs. 2b and c) but the temperature of the MoO_3 to MoO_2 reduction as well as the average H_2O concentration during reaction increases as the temperature ramping rate is increased to 1.0 K/min and subse-

TABLE 4

Syntheses with H_2O Added to N_2/H_2 Feed Stream

Sample	Feed gas water content	Average effluent water content[a]	Surface area	Temperature	Compound
WC03	276 ppm	1320 ppm	115. m^2/g	933 K	γ-Mo_2N
WC04	444 ppm	1500 ppm	133. m^2/g	933 K	γ-Mo_2N
WC05	1095 ppm	3290 ppm	97.2 m^2/g	933 K	γ-Mo_2N
WC06	1294 ppm	3440 ppm	63.4 m^2/g	933 K	γ-Mo_2N
WC07	2782 ppm	4390 ppm	49.5 m^2/g	933 K	γ-Mo_2N/Mo
WC08	3243 ppm	7190 ppm	24.0 m^2/g	933 K	γ-Mo_2N/Mo
WC09	20750 ppm		5.4 m^2/g	933 K	MoO_2/Mo

[a] Average water content during reduction obatined by averaging measured effluent water concentration from the onset of MoO_3 reduction until the end of temperature-programmed reaction.

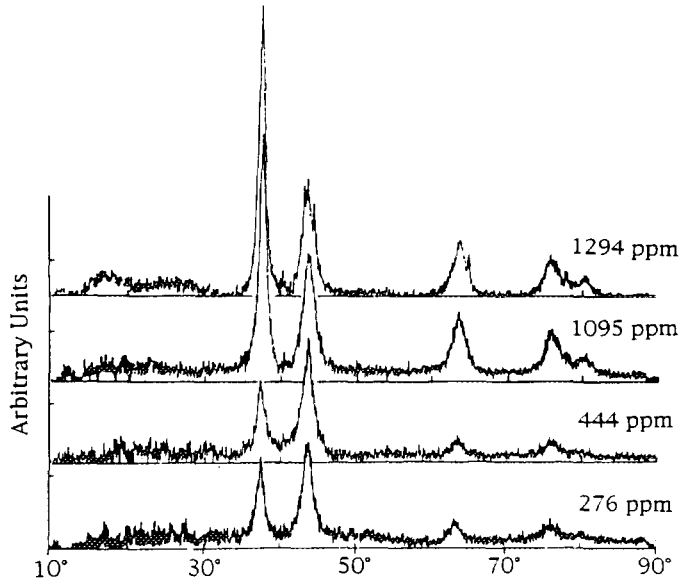

FIG. 1a. X-ray diffraction profiles of products from syntheses with water added to feed gas, water contents from 276 to 1294 ppm.

quently to 2.0 K/min (Table 2). The average effluent water concentration during reduction increases because reduction occurs over a shorter temperature interval and at a faster temperature ramping rate.

Evolution of Solid Structure

Table 5 illustrates changes in solid composition during temperature programmed reaction using the best known synthesis conditions (5/1 H_2/N_2 ratio, 260,000 hr^{-1} space velocity, and a temperature ramping rate of 0.6 K/min). For each sample, the temperature program was stopped at the indicated temperature and the reactor was rapidly cooled to room temperature. All samples were passivated prior to analysis. Particle sizes determined from surface area and X-ray data are shown in Table 6. It is noted that particle sizes determined by these methods only match for pure sample of spherical crystals. Differences indicate that the sample is impure, contains amorphous material, or consists of nonspherical crystals.

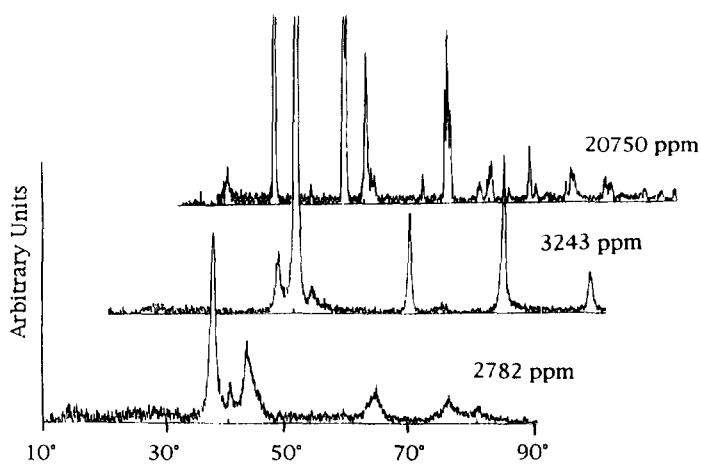

FIG. 1b. X-ray diffraction profiles of products from syntheses with water added to feed gas, water contents from 2782 to 20,750 ppm.

The X-ray diffraction profile of the MoO_3 starting material matches the positions and relative intensities given by the JCPDS file for MoO_3 (15). No traces of impurities were observed. No change in composition was observed by X-ray diffraction during temperature programmed reaction up to 573 K. Identical products are obtained when temperature programmed reaction begins at either 298 or 573 K, provided the reactor was purged of O_2 before heating to 573 K.

The reduction of MoO_3 to MoO_2 occurs between 573 and 673 K in this high space velocity reaction. At 673 K, only MoO_2 is observed by X-ray diffraction. BET analysis of the MoO_2 intermediate indicates an increase in specific surface area to 58.6 m^2/g. The crystallite size calculated from the MoO_2 X-ray peak width (43.3 nm) agrees poorly with the particle size estimated from BET surface area (15.8 nm), indicating that high surface area amorphous materials must also be present.

At 773 K (Fig. 3), the X-ray diffraction pattern is dominated by a large, wide peak corresponding to a lattice spacing of 205 nm (unknown intermediate I205) along with smaller peaks due to MoO_2. The calculated particle diameter of MoO_2 from the X-ray data is 69.7 nm, again in poor agreement with the value of 11.8 nm from surface area data and suggesting that high surface area amorphous material is present. The peak at 205 pm actually consists of a family of closely spaced reflections, and peak widths could not be accurately determined from the data. Interestingly, if the MoO_2/I205 mixture is held at 773 for 14 hr, the I205 is completely consumed and only MoO_2 is observed.

Between 773 K and 873 K, the sample is reduced to γ-Mo_2N. The X-ray diffraction pattern for the 873 K sample does not manifest peaks other than those of γ-Mo_2N. The surface area is on the order of 110 to 115 m^2/g. At 933 K, no further change in composition is observed by X-ray diffraction, yet the passivated product specific surface area increases to 150 m^2/g. If the reaction is allowed to continue to 980 K (the optimum high temperature in the previous NH_3 reactions), decreases in specific surface areas are observed. In our experiments, the γ-Mo_2N particle dimensions in both the [111] and [200] directions are a minimum at 893 K.

Scanning electron microscopy was used to investigate the solid morphology during reaction. The characteristic platelet morphology of MoO_3 is evident in electron micrographs of the starting material (Fig. 4). Platelets are nor-

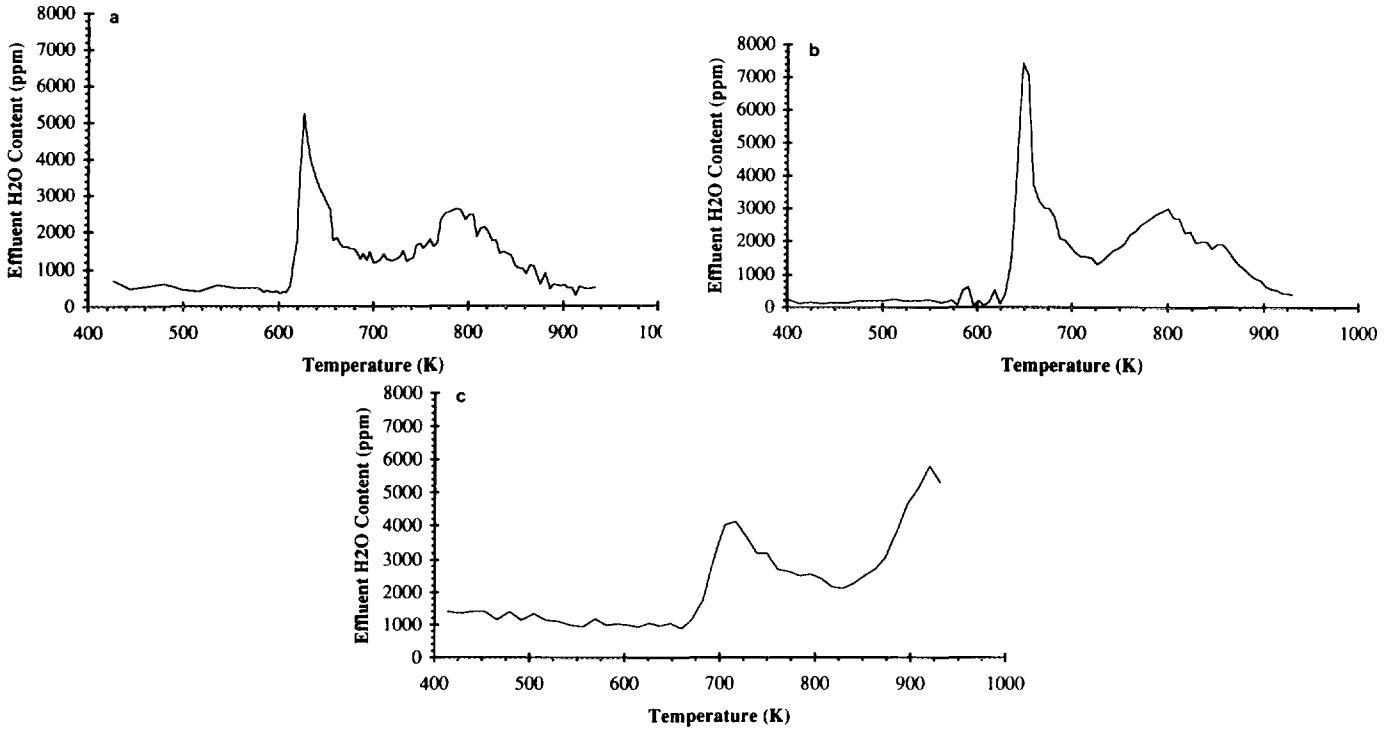

FIG. 2. Off-gas water content during syntheses of Mo_2N: (a) temperature ramp of 0.6 K/min; (b) temperature ramp of 1.0 K/min; (c) temperature ramp of 2.0 K/min.

mal to the [010] direction, leading to exaggerated [020] X-ray peak intensities when the platelets arrange anisotropically in the X-ray sample holder (2). The platelet habit was removable by grinding with a mortar and pestle, as previously reported (2).

SEM shows that the MoO_2/I205 and γ-Mo_2N reaction products are isomorphous to the reactant MoO_3 (Figs. 5, 6). The platelet morphology is observed in both product structures. The fine porosity of the high surface area materials, with features on the order of nanometers in size, could not be resolved using scanning electron microscopy. To compare the morphologies of topotactic and nontopotactic samples, micrographs of γ-Mo_2N and intermediate MoO_2 from reactions at elevated H_2O feed concentrations are included (Figs. 7, 8). These low surface area samples consisted largely of small granules approximately 1 μm in diameter or smaller, although some relics of platelet structure remain in the MoO_2 sample.

In order to obtain more information about the effect of space velocity on surface area generation, reactions with

TABLE 5

Evolution of Solid Structure during Temperature Programmed Reaction at 0.6 K/min

Sample	Temperature	Surface area	Composition	Pore volume
EV01	Starting material	2.0 m^2/g	MoO_3	.00477 cc/g
EV02	473 K	2.0 m^2/g	MoO_3	
EV03	573 K	2.0 m^2/g	MoO_3	
EV04	673 K	58.6 m^2/g	MoO_2	.0430 cc/g
EV05	773 K	78.6 m^2/g	MoO_2/I205[a]	
EV06	873 K	115. m^2/g	γ-Mo_2N	.0585 cc/g
EV07	893 K	111. m^2/g	γ-Mo_2N	.130 cc/g
EV08	933 K	151. m^2/g	γ-Mo_2N	.0959 cc/g
EV09	980 K	105. m^2/g	γ-Mo_2N	.0730 cc/g

[a] I205 was completely consumed when held at 773 K for 14 hr.

TABLE 6

Evolution of Average Particle Size during Temperature Programmed Reaction

Sample	Temperature	D_{hkl}, from Scherrer	D_p, from $6/pSg$
EV04	673 K	43.3 nm [011] MoO_2	15.8 nm
EV05	773 K	69.7 nm [011] MoO_2	11.8 nm
EV06	873 K	10.9 nm [111] γ-Mo_2N 7.21 nm [200] γ-Mo_2N	5.50 nm
EV07	893 K	7.93 nm [111] γ-Mo_2N 6.15 nm [200] γ-Mo_2N	5.69 nm
EV08	933 K	11.4 nm [111] γ-Mo_2N 7.73 nm [200] γ-Mo_2N	4.19 nm

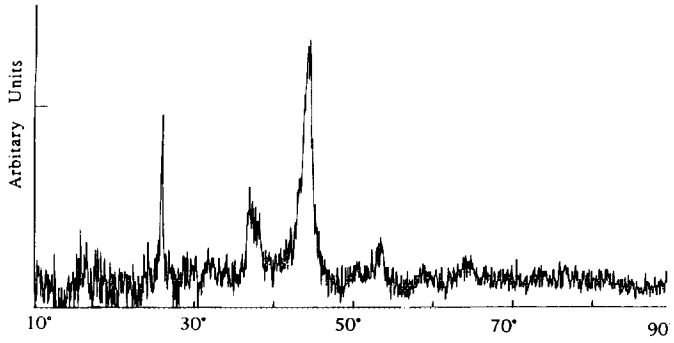

FIG. 3. X-Ray diffraction profile of intermediate MoO_2 and unknown compound (I205) observed at 773 K.

a range of space velocities (sample series SVI, Table 7) were stopped at 773 K to examine the structure of the primary reaction intermediates, MoO_2 and I205. The temperature ramping program was identical to that used in Series EV and SVF. As shown in Table 7, the surface area of the intermediate product increased with the total space velocity. I205 was not present in sample SVI04, prepared at low space velocity.

FIG. 4. Scanning electron micrograph of reactant MoO_3.

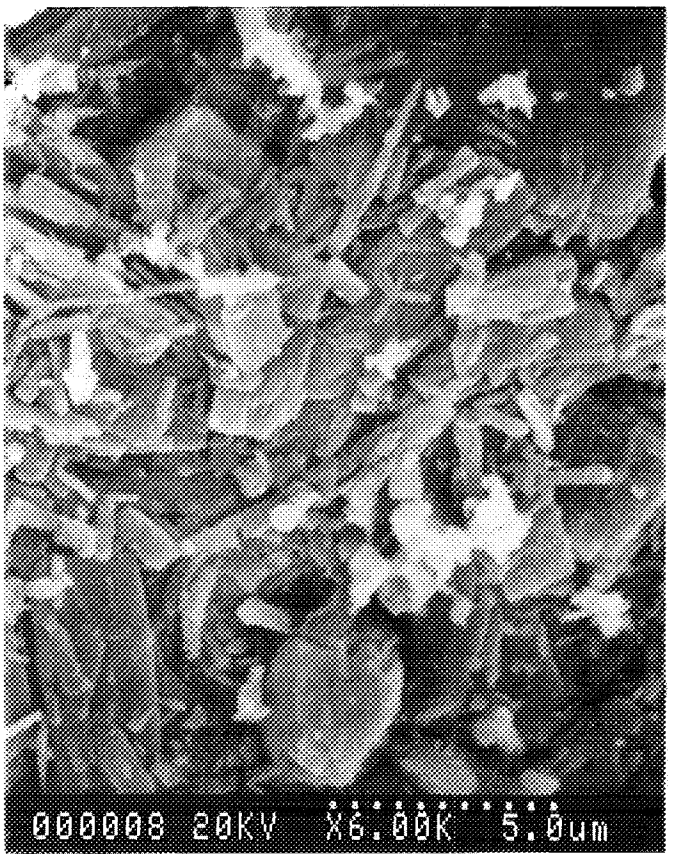

FIG. 5. Scanning electron micrograph of moderate surface area MoO_2.

DISCUSSION

General Observations

The primary result of this work is the production of very high surface area topotactic γ-Mo_2N (150 m^2/g) from MoO_3 in mixtures of N_2 and H_2. All previously reported syntheses involved reaction of NH_3 and MoO_3. In addition, this surface area is higher than the highest observed by us in NH_3 reactions (120 m^2/g, passivated) although others have reported higher surface areas in NH_3 syntheses (170 m^2/g, passivated (2)).

The use of N_2 and H_2 as reactants offers several advantages over the NH_3 synthesis for the large-scale production of topotactic γ-Mo_2N. First, reproducible surface areas of 150 m^2/g (passivated) are achieved. Second, virtually 100% of the synthesis gas may be economically recycled by drying. Third, while both synthesis methods involve the handling of dangerous and potentially explosive gases, the elimination of NH_3 from the flow system greatly simplifies fluid handling procedures as well as potential problems involving materials of construction. Last, the use of N_2/H_2 mixtures eliminates the heat transfer prob-

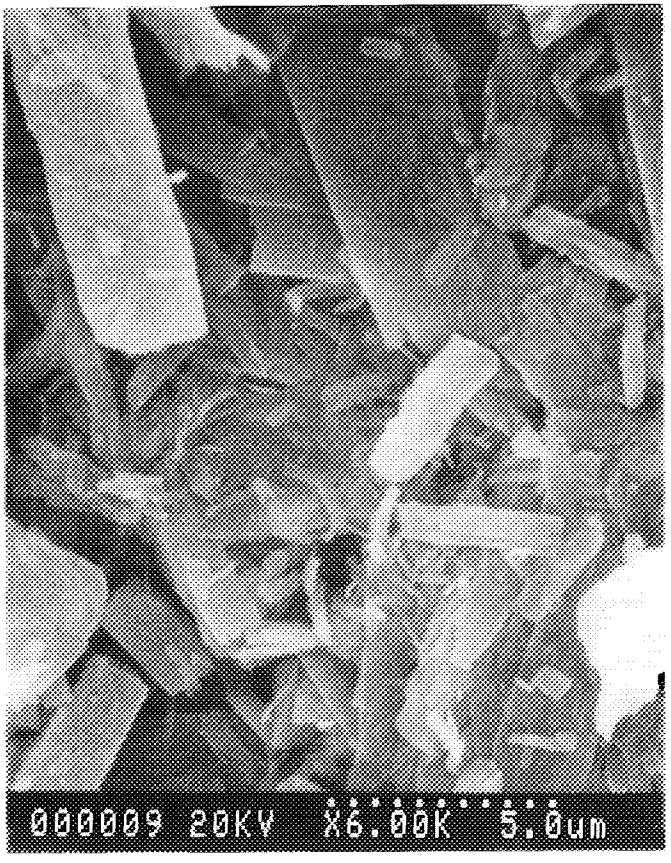

FIG. 6. Scanning electron micrograph of high surface area γ-Mo_2N.

lems associated with the endothermic decomposition of NH_3 in a large reactant bed. The decomposition reactions can interfere with the slow temperature programmed reaction and make large-scale syntheses untenable (9).

The observation that high surface area Mo_2N may be synthesized in N_2/H_2 mixtures is important to the understanding of the NH_3 reaction. We have previously shown that NH_3 decomposes at elevated temperatures during the synthesis of γ-Mo_2N (9) and it was proposed that depletion of NH_3 in the MoO_3 bed (primarily by catalytic decomposition) could be responsible for reactions yielding low surface areas. Our present results show that high surface areas may be obtained in the complete absence of NH_3, but that added H_2O leads to lower surface areas.

The evolution of high surface area with temperature, conservation of the MoO_3 platelet morphology (Fig. 6), and exaggerated [200] Mo_2N X-ray peaks observed in the product of the N_2/H_2 reaction are also observed in the NH_3 reduction. On this basis, we conclude that the N_2/H_2 reduction reaction follows a topotactic route as well, although electron diffraction data for a single particle is required to prove the topotactic nature of the N_2/H_2 reaction. The effects of space velocity and temperature ramping rate are also similar to those observed in the topotactic reduction of MoO_3 in NH_3 (1, 2). A significant difference between the two syntheses is the observation that the surface areas of MoO_2 intermediates in N_2/H_2 reactions are much higher than in the corresponding NH_3 reactions. In addition, formation of Mo_2N is observed much earlier during temperature programmed reaction in N_2/H_2 (2).

Effects of Reaction Variables on Surface Area

Samples SVF, TRR, and WC show that low surface areas are produced in syntheses with low space velocities, high temperature ramping rates, and high water contents. GC analysis of the reactor effluent during reactions at different temperature ramping rates (Table 2) indicates that higher ramping rates lead to higher H_2O concentrations. In addition, a mass balance on the reactant bed shows that lower space velocities lead to higher effluent H_2O concentrations. Thus, it is possible that reactions with low space velocities and high temperature ramping rates yield low surface areas due to the high concentrations of H_2O present during reaction. To illustrate this linkage, the average H_2O effluent concentrations observed (between temperatures of 573 K and 933 K) for

FIG. 7. Scanning electron micrograph of low surface area MoO_2 formed when high levels of H_2O are present in gas stream.

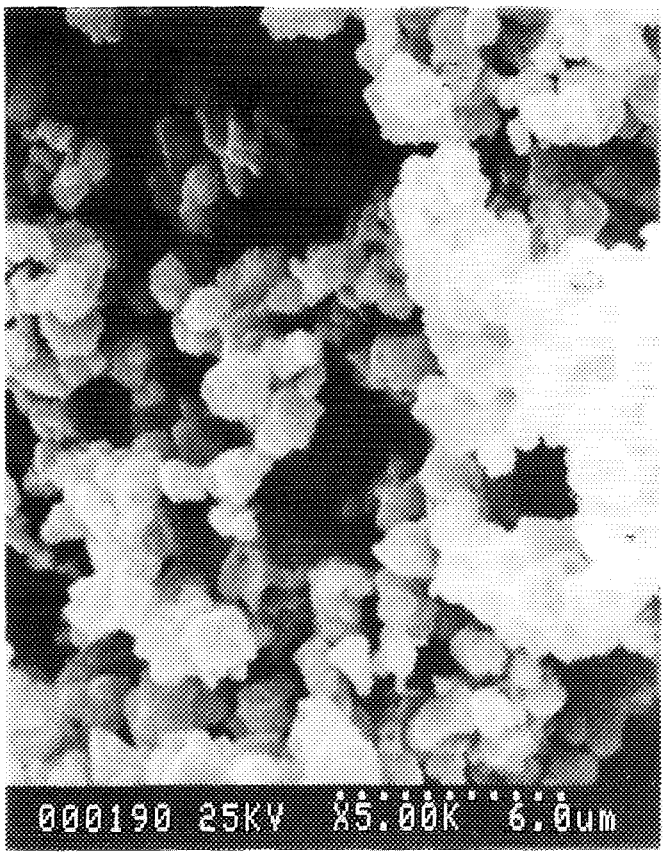

FIG. 8. Scanning electron micrograph of low surface area γ-Mo_2N formed when high levels of H_2O are present in gas stream.

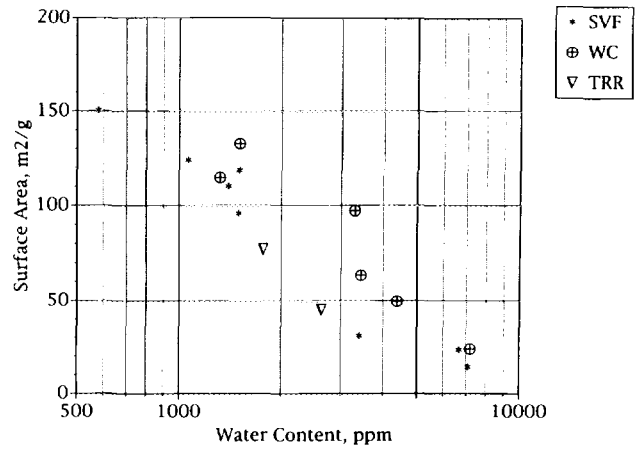

FIG. 9. Relationship of product specific surface area and average effluent water content in syntheses with different temperature programs, water contents, and space velocities.

experiments SVF, TRR, and WC are plotted versus product surface areas in Fig. 9. From the figure, a correlation can be seen between resultant product surface area and average water content in the bulk gas for a wide range of reaction conditions.

One mechanism which may be responsible for the loss of surface area is hydrothermal sintering. In hydrothermal sintering, volatile metal oxide hydrates form (as observed experimentally in this work and previously reported (11, 16)) in the presence of water. The increased mobility of the hydrate species leads to aggregation of the reacting solids and lower surface areas.

TABLE 7

Space Velocity Effects on Intermediate Structures Observed at 773 K

Sample	H_2	Space velocity	Surface area m^2/g	Composition
SVI01	84.3%	255,000 hr^{-1}	78.6	MoO_2/I205
SVI02	85.2%	84,300 hr^{-1}	60.7	MoO_2/I205
SVI03	85.0%	68,100 hr^{-1}	64.0	MoO_2/I205
SVI04	81.1%	22,800 hr^{-1}	33.4	MoO_2

Another mechanism which may account for reduced surface areas is lattice fluidization. In this mechanism, elevated temperature causes increased mobility of metal atoms in the lattice. This disruption of the Mo lattice disrupts the topotactic nature of the desired reactions and interferes with the development of pores and surface area. Lattice fluidization is expected to occur at temperatures on the order of 60% of the solid melting point (11), which for MoO_3 is 640 K. While MoO_2 and γ-Mo_2N are expected to be stable throughout reaction, MoO_3 and unstable reaction intermediates may fluidize so that desirable nanostructure is lost (19). Our data regarding the effects of H_2O on surface area generation indicate that higher H_2O concentrations accompany higher reduction temperatures. For this reason, lattice fluidization can account for the effects of H_2O concentrations, temperature ramping rate, and space velocity on Mo_2N surface area.

Two known effects can explain how increased H_2O concentrations can lead to higher reduction temperatures: slowed reaction kinetics and thermodynamically unfavorable reaction conditions. Kinetic effects which may lead to delayed reduction include competitive adsorption of H_2O over H_2 (as observed by Hillis *et al.* (12)) and solid state diffusion limited mass transfer of either H_2 into or oxygen containing species out of a hydrothermally sintered Mo lattice (consistent with the observation that the activation energy of reaction is characteristic of solid state diffusion (6, 20)). Alternatively, a thermodynamic analysis indicates that elevated levels of H_2O increase molybdenum dioxide reduction temperatures, consistent with Le Chatelier's Principle (Fig. 10).

Thermodynamic Analysis

Equilibrium diagrams (Fig. 10) showing the effect of H_2O concentration and N_2/H_2 ratio on solid composition at equilibrium were calculated from tabulated thermody-

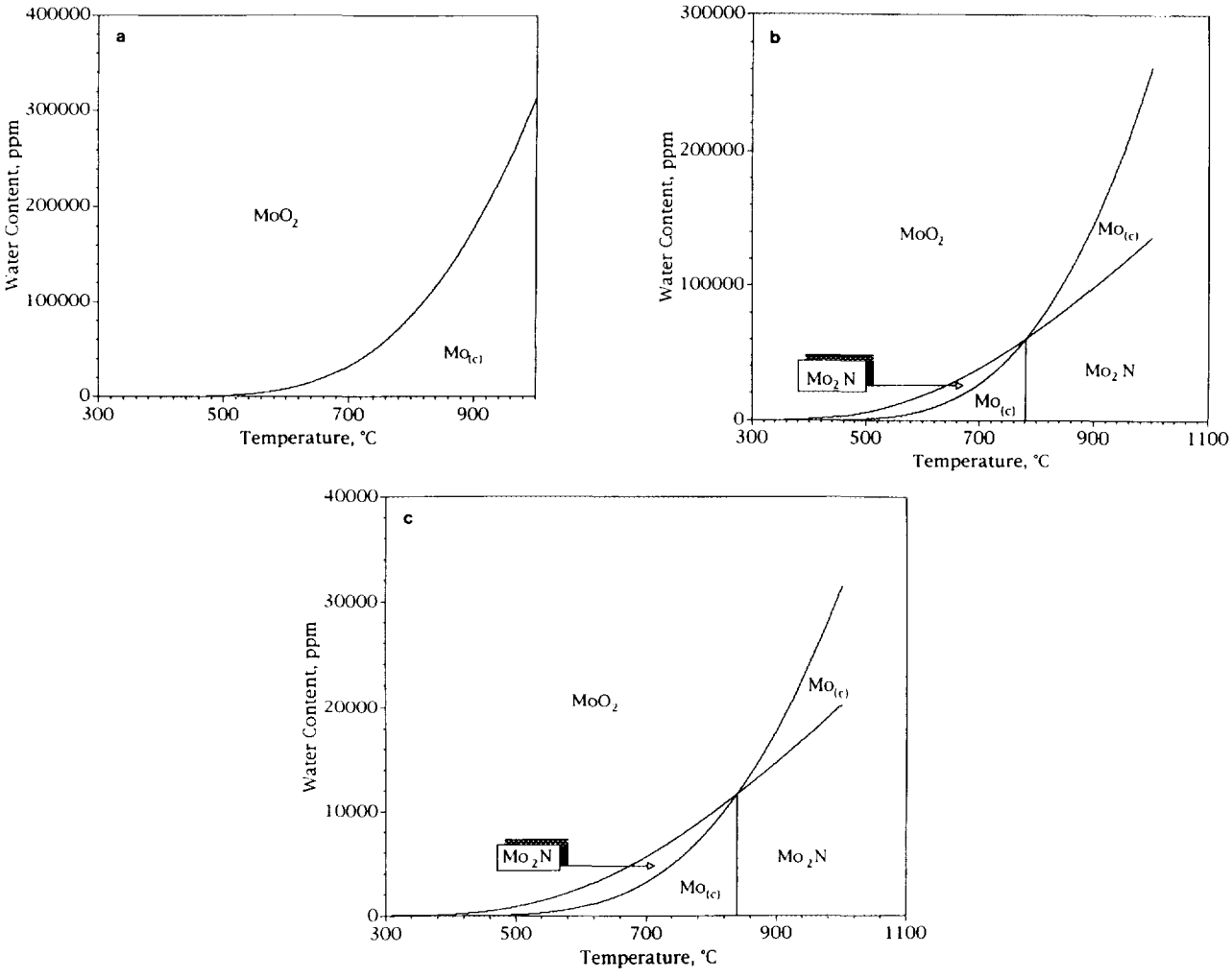

FIG. 10. $MoO_3/H_2/N_2$ reaction equilibrium diagrams: (a) N_2/H_2 ratio of 0.0; (b) N_2/H_2 ratio of 0.2; (c) N_2/H_2 ratio of 9.0.

namic data (19). Only two reactions were considered: the reduction of MoO_2 to Mo by H_2, and the nitridation of Mo to γ-Mo_2N (as well as the sum of these two reactions, $MoO_2 \rightarrow \gamma$-Mo_2N). Because no thermodynamic data are available for I205 and no other solid intermediates were observed, only MoO_2, Mo_2N, and Mo are included. Thus, these calculations represent a simplification of a reaction system which may include a number of other intermediate solid compounds, such as I205.

For all hydrogen-containing systems at the temperatures considered in this study, the presence of MoO_3 is strongly disfavored by equilibrium (18). Thus, the presence of MoO_3 in our syntheses is due to kinetic effects and changes in MoO_3 reduction temperatures must be ascribed to kinetic factors. However, calculations show that MoO_2 is expected at low temperatures in our reactions (with background H_2O concentrations generally above 200 ppm). The MoO_2 reduction temperatures are strongly influenced by the concentration of H_2O in the gas phase (Fig. 10). Lowest reduction temperatures are found in syntheses with low H_2O concentrations and low N_2/H_2 feed ratios. These are the same conditions shown to give the highest surface areas. However, the observed and calculated temperatures of reduction do not agree. For example, sample series EV shows that during the synthesis yielding highest surface area, MoO_2 is reduced between 773 K and 873 K, while equilibrium calculations indicate the reduction should take place at much lower temperatures. It is concluded that the MoO_2 reduction temperature is strongly influenced by kinetic factors, not equilibrium.

While kinetics influences which solid rection intermediates are observed, thermodynamics correctly predicts Mo_2N as the final product in most reactions. Interestingly, it is also predicted that MoO_2 is reduced to Mo before forming Mo_2N at the final reaction temperature. The intermediate metal phase was not directly observed experimentally, but the absence of Mo is consistent with the

observation that the reduction of MoO_2 does not commence until this region of the phase diagram is nearly past, due to kinetic effects. It may be possible to observe the intermediate metal phase at temperatures near 825 K.

In reactions involving high H_2O content, Mo and MoO_2 are observed at the final reaction temperature of 933 K instead of the Mo_2N predicted by equilibrium. Their presence is due to kinetic factors, possibly including limited mass transfer in the large crystallites of these low surface area materials. The presence of Mo is particularly interesting in these samples because the H_2O content of these reactions was never high enough to reach the upper (high temperature) Mo phase envelope. For this reason, the Mo present must have formed in the lower phase envelope, and been preserved as an artifact from the low temperature region by kinetic factors. Thus, the presence of Mo in sample series WC is indirect evidence of metallic intermediates in Mo_2N synthesis.

The presence of an Mo intermediate is also observed in sample PG02. Low surface area MoO_2, Mo_2N, and Mo are observed at 933 K when only Mo_2N is expected. The Mo and MoO_2 are artifacts formed at lower temperatures and preserved by slow reaction kinetics. It is believed that the slow reduction kinetics are the result of the large crystallite size and the resulting long path lengths for solid state diffusion. The preservation of Mo intermediates is not observed in similar syntheses (PG03, SVF04) which yield high surface area materials with an average path length for solid state diffusion of only a few nanometers.

Reductions in pure hydrogen yield high surface area Mo as expected from thermodynamics. Reduction to Mo occurs near 773 K, although much lower reduction temperatures are predicted by thermodynamics. The presence of I205 in sample PG04 produced by the reaction of MoO3 and pure H_2 is particularly interesting: this compound has previously been discussed as an oxynitride, but virtually no structural or composition data are reported to support this conclusion. The observation of I205 in this nitrogen-free synthesis indicates that it contains no nitrogen. Because only molybdenum, hydrogen, and oxygen were present in reaction PG04, it is likely the compound is a molybdenum oxide, hydroxide, or hydrate.

Additional information about compound I205 is provided by comparison of syntheses SVF, EV, and PG04. I205 is only observed in the presence of MoO_2, Mo, and Mo_2N. In addition, I205 is present in series EV only at the highest temperature at which MoO_2 is present before it is reduced to the final product. This data strongly suggests that I205 is an intermediate in the conversion of MoO_2 to Mo or Mo_2N. However, it is also observed that I205 is consumed at 773 if allowed time for reaction (EV05), but without any Mo or Mo_2N being formed. Additional work is required to ascertain the role of I205 in the reduction mechanism.

Solid Structures

Surface area is generated during the reduction of MoO_3 to MoO_2 and during the reduction of MoO_2 to final products. Syntheses with 3000 ppm H_2O in the N_2/H_2 feed produced very low surface area MoO_2 (sample WC02) at 773 K, but during the subsequent reduction of low surface area MoO_2 to γ-Mo_2-N, surface areas increased to 49.5 m^2/g (sample WC07). Thus, we conclude that the evolution of surface area occurs during both the MoO_3 to MoO_2 transformation and the MoO_2 to γ-Mo_2N transition and that H_2O affects the MoO_3 reduction reaction more strongly at these H_2O concentration levels.

Particle sizes calculated from X-ray linewidth data and surface area data (Table 6) generally did not match well, indicating the presence of amorphous material. The discrepancies are largest in low temperature samples consisting of large MoO_2 crystallites and high surface area amorphous material. While particle sizes calculated from surface area generally increase throughout reaction to 933K, D_{hkl} goes through a minimum at 893 K. Sintering of Mo_2N is observed upon heating from 893 to 933 K while surface areas increase, perhaps by the conversion of amorphous materials to high surface area Mo_2N.

When the N_2/H_2 reaction yielding maximum surface area was halted at 673 K, the passivated solid reaction product consisted entirely of moderate surface area MoO_2 (sample EV04). Interestingly, only low surface area MoO_2 is observed in equivalent NH_3 syntheses (2, 9). Bertrand and Dufour (11) have discussed in detail the topotactic reduction of MoO_3 to MoO_2 in flowing H_2. They determined that the transformations occurred layer by layer, with either H_2O or OH radicals diffusing out along structural holes in the [100] direction of MoO_2 ([010] direction of MoO_3). The low synthesis temperature of our MoO_2 (673 K) is within the range of reaction temperatures used by Bertrand and Dufour for topotactic MoO_2 synthesis in H_2. As expected for topotactic reaction, we observed conservation of the platelet morphology for the high surface area intermediate. Particle sizes calculated from the Scherrer equation using [011] MoO_2 X-ray reflections (Table 6) and surface area data are of the same order, but are not equal. For a platelet morphology, the characteristic length of D_{200} should be $\frac{2}{3}$ that of D_p calculated for spherical particles (18), but this is not observed (Table 6). The presence of an amorphous compound may account for this discrepancy, but IR spectra of I205/MoO_2 mixtures showed only peaks due to MoO_2 (14).

The increase in pore volume during the transformation from MoO_3 to MoO_2 is approximately 50% of the value expected if the transformation occurred with no change in external morphology and crystallite size. This indicates that external particle dimensions are not preserved during the topotactic N_2/H_2 reaction. However, other effects

may also account for this discrepancy: the crystallite size is on the order of 10 nm, and deep, small radius pores may exist which are too narrow for the N_2 molecule to penetrate. This is evident in the NH_3/MoO_3 reaction from BET analysis (2), where there was a dramatic increase in the normalized pressure (P/P_S) needed for monolayer completion of the 980K (γ-Mo_2N) sample relative to the 835 K intermediate. In addition, as much as 25% of the pore volume is expected to be lost during passivation in air, similar to the loss seen in products of NH_3 reduction (2). It is also possible that an amorphous oxide phase with density between MoO_2 and MoO_3 is present in EV04.

Mo is observed in a number of instances as a final product during syntheses containing high levels of H_2O (WC07-WC09), dilute mixtures of H_2 in N_2 (PG02), and pure H_2 (PG04, PG06). Particle sizes by the Scherrer equation are small (suggesting high surface areas) for Mo formed in dry H_2 syntheses, whereas a large particle diameter (suggesting low surface areas) is calculated for Mo formed in high levels of H_2O. The formation of moderate surface area topotactic Mo was previoulsy reported (4) in dry hydrogen syntheses. Mo is the thermodynamic product expected for 773 K $H_2/N_2/MoO_3$ syntheses in which the N_2 partial pressure is below 30 Torr (Fig. 10) or the water content is less than 21.8%. In dry syntheses, moderate surface area Mo is rapidly nitrided at elevated N_2 partial pressures to produce high surface area γ-Mo_2N (12) but the presence of H_2O inhibits the uptake of nitrogen by Mo (12).

CONCLUSIONS

MoO_3 may be reduced to high surface area γ-Mo_2N (150 m^2/g) by temperature programmed reduction in mixtures of N_2 and H_2. The use of N_2 and H_2 as reactants offers several advantages over the NH_3 synthesis for the large-scale production of topotactic γ-Mo_2N: reproducible surface areas of 150 m^2/g (passivated) are readily achieved, virtually 100% of the synthesis gas may be economically recycled by drying and the heat transfer problems associated with the endothermic decomposition of NH_3 in a large reactant bed are eliminated. In addition, the elimination of NH_3 from the flow system greatly simplifies fluid handling procedures as well as potential materials of construction problems.

The surface area achieved in the final product is strongly dependent on the average H_2O concentration in the gas phase during reaction. Thus, very high gas space velocities and slow temperature ramping rates are required to remove the water produced by the reduction reactions. Loss of surface area is attributed to either hydrothermal sintering or lattice fluidization at elevated temperatures. Elevated reduction temperatures are observed in syntheses with high H_2O effluent concentrations. A thermodynamic analysis indicates the reduction temperatures are determined by kinetic factors, not reaction equilibria. Due the absence of film diffusion effects, reaction kinetics are determined by the rate of solid state diffusion of oxygen and nitrogen in the lattice as well as by competitive adsorption effects involving H_2O and H_2.

In contrast to the NH_3 synthesis, high surface area intermediate MoO_2 is observed. An unidentified molybdenum oxide, hydroxide, or hydrate is also observed as an intermediate in many syntheses. Thermodynamic calculations indicate that metallic molybdenum should form as an intermediate in N_2/H_2 syntheses, but usually none is observed due to slow reduction kinetics in the region where Mo is expected. No intermediates are observed by adding H_2O to the N_2/H_2 mixture, thereby elevating the temperature range over which Mo is expected.

ACKNOWLEDGMENTS

This work was supported by the College of Engineering and the Department of Chemical Engineering at the University of South Carolina. One of us (RSW) thanks the Carolina Eastman Company for a graduate research fellowship.

REFERENCES

1. Markel, E. J., and Van Zee, J. W., *J. Catal.* **126,** 643 (1990).
2. Volpe, L., and Boudart, M., *J. Solid State Chem.* **59,** 332 (1985).
3. Volpe, L., and Boudart, M., *J. Phys. Chem.* **90,** 4878 (1986).
4. Ranhotra, G. S., Bell, A. T., and Reimer, J. A., *J. Catal.* **108,** 40 (1987).
5. Schlatter, J. C., Oyama, S. T., Metcalf, J. E., and Lambert, J. M., *Ind. Eng. Chem. Res.* **27,** 1648 (1988).
6. Oyama, S. T., and Sajkowski, D. J., *Prepr. Am. Chem. Soc. Div. Pet. Chem.* **35** (2), 233 (1990).
7. Pickett, W. E., Klein, B. M., and Papaconstantopoulos, P., *Physica B* **107,** 667 (1981).
8. Lide, D. R.,"CRC Handbook of Chemistry and Physics." CRC Press, Ann Arbor, MI (1990).
9. Wise, R. S., and Markel, E. J., *J. Catal.* **145,** 335 (1994).
10. Anderson, J., *J. Phys. Suppl.* **38,** C7–17 (1977).
11. Bertrand, O., and Dufour, L. C., *Phys. Status Solidi A* **60,** 507 (1980).
12. Hillis, M. R., Kemball, C., and Roberts, M. W., *Trans. Faraday Soc.* **62**(12), 3570 (1966).
13. King, E. G., Weller, W. W., and Christensen, A. U., U.S. Bureau of Mines, Report. 1960.
14. Wise, R. S., and Markel, E. J., unpublished results.
15. "JCPDS X-Ray Powder Diffraction Inorganic Reference Data." 1987.
16. Bertrand, O., and Dufour, L. C., *C.R. Seances Acad. Sci. Ser. C* **278,** 315 (1974).
17. Klug, H. P., and Alexander, L. E., "X-Ray Diffraction Procedures," Chap. 9. Wiley, New York, 1962.
18. Wise, R. S., M. S. Thesis. University of South Carolina, 1992.
19. Chase, M. W., Davies, C. A., Downey, J. R., Frurip, D. J., McDonald, R. A., and Syverud, A. N., "JANAF Thermochemical Tables," 3rd ed.
20. Schlatter, J. C., Oyama, S. T., Metcalf, J. E., and Lambert, J. M., *Ind. Eng. Chem. Res.* **27,** 1639 (1988).